

ARTICLE

Open Access

# Aptamer-functionalized smart photonic hydrogels: application for the detection of thrombin in human serum

Peiyan Shen<sup>1</sup>, Mengru Li<sup>1</sup>, Ran Li<sup>1</sup>, Bo Han<sup>1</sup>, Haojie Ma<sup>1</sup>, Xueyan Hou<sup>1</sup>, Yuqi Zhang<sup>1</sup> and Ji-Jiang Wang<sup>1</sup>

## Abstract

Smart photonic hydrogels based on two-dimensional photonic crystals (2DPC) provide a promising sensing platform for constructing novel chemical and biological sensors due to their facile optical signal readout and highly sensitive responsivity toward target analytes. Aptamers, as recognition elements with high selectivity and affinity, are extensively used to construct a variety of sensors. Herein, we developed two partially base complementary aptamer-functionalized 2DPC hydrogels as aptasensors for the detection of thrombin (TB) in human serum. The photonic hydrogel aptasensors swelled upon exposure to TB solution, leading to an increase in the particle spacing of the 2DPCs. The particle spacing changes were acquired by simply measuring the diameters of the Debye ring diffracted by the 2DPCs without the requirement of sophisticated instruments. The aptasensor swelling resulted from the decrease in the hydrogel cross-linking density induced by the specific binding between one of the aptamers and TB and the increase in hydrogel mixing free energy induced by the introduction of TB. The particle spacing increase of the optimized aptasensor was linear over the TB concentration range of 1–500 nM, and the limit of detection was 0.64 nM. The constructed 2DPC hydrogel aptasensor was used to detect TB in human serum and achieved recoveries of 95.74–104.21% and a relative standard deviation of 2.52–6.58%, showing the practicability and accuracy of the sensor. The aptamer-actuated 2DPC hydrogel biosensor provides a new strategy for designing other target molecule-sensitive aptasensors, showing great potential for development into home kits.

## Introduction


Smart photonic hydrogels are promising candidates for developing novel chemical and biological sensors due to their facile optical signal readout and highly sensitive responsivity toward target analytes<sup>1,2</sup>. Two-dimensional photonic hydrogels are fabricated by embedding a two-dimensional photonic crystal (2DPC) into a polymer hydrogel network<sup>3</sup>. A 2DPC, as an optical material, is composed of two dielectric substances with different refractive indices and shows strong light diffraction in the forward direction due to its periodic array structure<sup>4</sup>. A 2DPC array diffracts

light at an angle and forms a bright ring defined as a Debye ring when it is irradiated by monochromatic incident light<sup>5,6</sup>. The diameter of the Debye diffraction ring reflects the particle spacing of the 2DPC<sup>7</sup>. Smart hydrogels are soft materials that can respond to external stimuli and generate volume phase transitions<sup>8</sup>. When a 2DPC array is embedded in a smart hydrogel, the particle spacing of the 2DPC will change after the hydrogel is exposed to an environment containing target analytes due to the hydrogel volume change induced by the external stimuli. These particle spacing changes can be used as sensing signals for external stimuli and can be acquired by measuring the Debye diffraction ring diameter with just a laser pointer and a ruler and without sophisticated instruments<sup>1,9–11</sup>. Thus, smart 2DPC hydrogels (2DPCH) are considered an ideal and

Correspondence: Yuqi Zhang (yqzhang@yau.edu.cn)

<sup>1</sup>Key Laboratory of New Energy & New Functional Materials, Shaanxi Key Laboratory of Chemical Reaction Engineering, College of Chemistry and Chemical Engineering, Yan'an University, Yan'an, Shaanxi 716000, P. R. China

© The Author(s) 2022

 **Open Access** This article is licensed under a Creative Commons Attribution 4.0 International License, which permits use, sharing, adaptation, distribution and reproduction in any medium or format, as long as you give appropriate credit to the original author(s) and the source, provide a link to the Creative Commons license, and indicate if changes were made. The images or other third party material in this article are included in the article's Creative Commons license, unless indicated otherwise in a credit line to the material. If material is not included in the article's Creative Commons license and your intended use is not permitted by statutory regulation or exceeds the permitted use, you will need to obtain permission directly from the copyright holder. To view a copy of this license, visit <http://creativecommons.org/licenses/by/4.0/>.

facile sensing material by monitoring their Debye diffraction rings to detect target analytes.

Presently, a variety of sensors based on smart 2DPC hydrogels have been developed for detecting different target analytes, such as  $\text{H}_2\text{O}_2$ <sup>12</sup>,  $\text{Ag}^+$ <sup>13</sup>, urea<sup>14</sup>, glucose<sup>15,16</sup>, amino acids<sup>13,17</sup>, proteins<sup>18,19</sup> and microorganisms<sup>20–22</sup>. For example, Cai et al.<sup>12</sup> developed a label-free 2DPC protein hydrogel for the colorimetric detection of  $\text{H}_2\text{O}_2$ . A urea and urease inhibitor sensor<sup>14</sup> was constructed by introducing urease into a 2DPCH as a recognition element. Recently, aptamer-crosslinked 2DPCH have been reported to detect  $\text{Ag}^+$ , Cys and SARS-Corona viruses<sup>13,22</sup>. Inspired by these works, the design and construction of simple, highly sensitive and selective 2DPCH sensors for detecting proteases in body fluids is promising.

Proteases, which play crucial roles in many pathological and physiological processes, can participate in and regulate many physiological activities and act as biomarkers for some diseases<sup>23</sup>. For example, thrombin (TB) can serve as a potential diagnostic biomarker because it is involved in some diseases, such as Alzheimer's disease<sup>24</sup>, nephrotic progression<sup>25</sup>, venous thromboembolism<sup>26</sup> and cancers<sup>27</sup>. Using various analytical techniques, many of the developed TB-sensitive materials, especially aptamer-based biosensors, have realized the effective detection of TB<sup>28–30</sup>. Aptamers are single-stranded DNA or RNA that can bind target molecules with high selectivity and affinity<sup>31</sup>. They are widely used to construct various aptasensors, including TB-sensitive sensors through the introduction of TB-binding aptamers<sup>32</sup>, due to their simple synthesis, high stability, diversified design, easy modification, and low cost<sup>33,34</sup>. For example, Zboril and coworkers<sup>28</sup> fabricated an aptamer-modified hierarchically porous fluorinated graphene oxide@metal–organic gel composite to detect TB with a limit of detection (LoD) of 58 pM using an electrochemical method. Hu et al.<sup>29</sup> reported a polymer brush modified by aptamers as a TB sensor and used the surface plasmon resonance technique to highly and sensitively recognize TB with an LoD of 1.1 nM in human blood plasma. These methods are reliable, selective, and sensitive, with LoDs that reach the pM or even fM scale<sup>30</sup>. However, their practical and clinical applications are restricted by time-consuming, complicated sample preparation and bulky, expensive instruments. Therefore, developing 2DPCH aptasensors is a promising strategy for the construction of TB-sensitive sensors to achieve the simple, low-cost and clinically applicable detection of TB.

In this work, we constructed two partially base complementary aptamer-functionalized 2DPCH sensors to accurately detect TB in human serum. Amino-terminated DNA aptamers were linked into a carboxyl-rich hydrogel network containing a polystyrene 2DPC array by amide

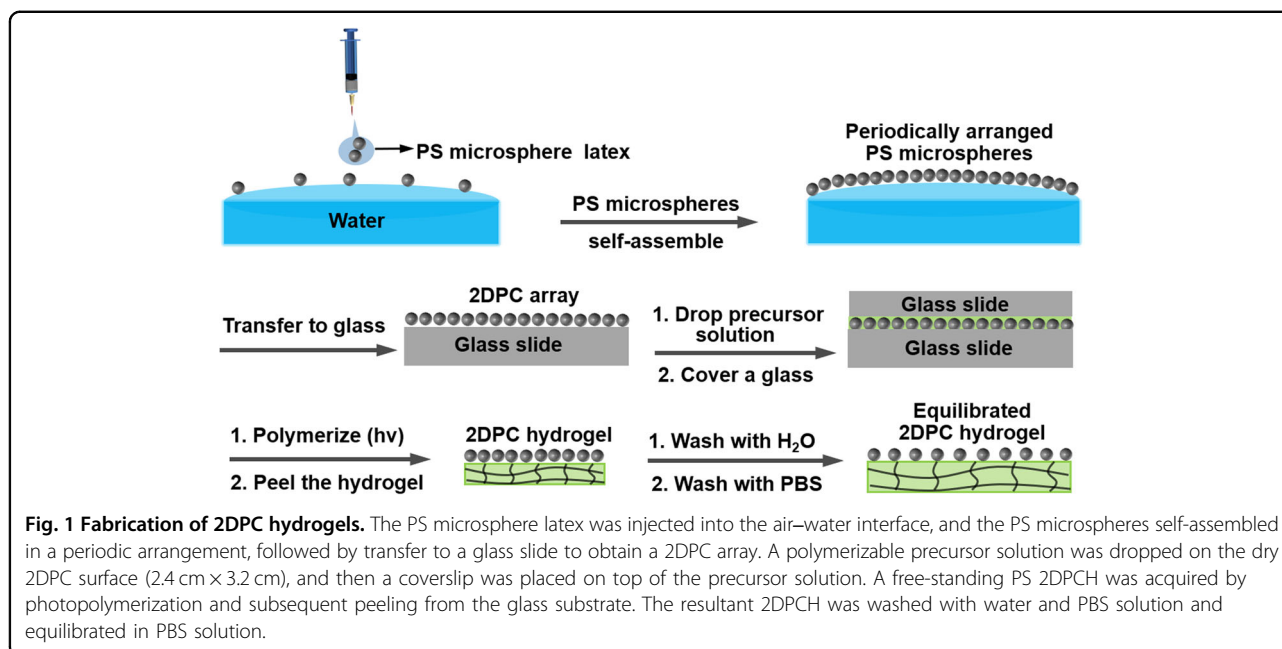
bonds. Upon exposure to TB solution, the photonic hydrogel aptasensors swelled, and the particle spacing of the 2DPC embedded in the hydrogel networks increased. The reason for this is that the binding between TB and one of the aptamers opened the complementary bases of the DNA strands linked to the polymer chains, releasing the other aptamer and leading to a decrease in the cross-linking density of the hydrogel. Additionally, the introduction of TB molecules into the aptasensors induced an increase in the mixing free energy of the hydrogel. The 2DPCH aptasensors were used to detect TB in human serum, and the results demonstrated their practicality and accuracy. This type of aptamer-actuated 2DPCH aptasensor is low-cost, simple, selective and sensitive, providing a new strategy for designing other protease-sensitive biosensors.

## Experimental section

### Materials and characterization

Human thrombin ( $\geq 2000$  units/mg), bovine serum albumin (BSA), human albumin (Alb) and adenosine (AD) were purchased from Sigma–Aldrich. Acrylic acid (AAc), acrylamide (AAm), N, N'-methylenebisacrylamide (Bis), 2-hydroxy-4'-(2-hydroxyethoxy)-2-methylpropiophenone (I<sub>2959</sub>), 1-ethyl-3-(3-dimethylaminopropyl) carbodiimide hydrochloride (EDC) and cysteine (Cys) were supplied by Aladdin Chemistry Co., Ltd. N-Hydroxysulfosuccinimide sodium salt (NHS) was purchased from J&K Scientific Co., Ltd. Lysozyme (Lys), the aptamer 5'-NH<sub>2</sub>-(CH<sub>2</sub>)<sub>6</sub>-ACTGTGGTTGGTGTGGTTGG (S1) and its partially complementary sequence 5'-NH<sub>2</sub>-(CH<sub>2</sub>)<sub>6</sub>-ACCAACCA CAGT (S2) were acquired from Sangon Biotech. Co., Ltd. Human serum was provided by Hefei Bomei Biotech. Co., Ltd. AAc was purified by distillation before use. Phosphate buffered saline (PBS) solution (10 mM, pH 7.40) was used for all measurements. Nanopure water (18.2 mΩ·cm) obtained from a Duro Pro 12FV water purification system was used to prepare all solutions. Polystyrene (PS) microspheres with a diameter of ~960 nm were synthesized by dispersion polymerization and then purified by repeated centrifugation and dispersion<sup>35</sup>. The diameter and particle size distribution of the PS microspheres were characterized by dynamic light scattering (DLS), as shown in Fig. S1a. The diameter of the PS microspheres was 964.8 ± 52.8 nm. Moreover, the diameter obtained by the SEM image (Fig. S1b) of the 2DPC prepared from these PS microspheres was 956 nm, which was close to the result from the DLS method. Thus, we characterized the PS microsphere diameter as ~960 nm.

The microstructures of the prepared 2DPC and 2DPCH were observed using a scanning electron microscope (SEM, JSM-7610F, JEOL, Japan) after gold sputtering. The FTIR spectra were recorded on a Fourier transform infrared spectrometer (FTIR, Nicolet iS5, US).



### Fabrication of the 2DPC hydrogel and measurement of the Debye diffraction ring

The PS microsphere latex (~20 wt%) was mixed with 1-propanol at a volume ratio of 3:1, followed by vortexing for 2 min. The mixture was slowly and smoothly injected into an air–water interface using a syringe (Fig. 1)<sup>36</sup>. The PS microspheres spread outward due to the difference in surface tension between water and 1-propanol and self-assembled to form a 2DPC monolayer array in a hexagonally close-packed arrangement on the water surface. The resultant 2DPC array was carefully transferred onto a glass slide (2.4 cm × 7.6 cm) and dried in air. Next, a certain volume of polymerizable precursor solution containing AAc, AAm, Bis and I<sub>2959</sub> was dropped onto the dry 2DPC array surface and then covered with a glass slide. The “sandwich” sample was irradiated by 365 nm UV light for 30 min to initiate the polymerization reaction to fabricate the 2DPC-P(AAm-co-AAc) hydrogel film (Scheme S1). The resulting 2DPC hydrogel film was peeled off the glass surface and immersed into ultrapure water for a thorough wash of 6 h (the water was changed every 2 h) to remove the unreacted monomers. The hydrogel was further immersed into PBS solution for 6 h (the PBS solution was changed every 2 h), followed by equilibration in PBS solution for 24 h. The equilibrated 2DPC hydrogel swelled to form a periodically nonclose-packed structure of PS microspheres because of the existence of the carboxyl groups in PBS solution at pH = 7.40.

The resultant 2DPC hydrogel could diffract a Debye ring on the bottom screen when illuminated by a laser along the array normal. This is because the 2DPC array shows strong forward diffraction, and the 2DPC array

domain has identical spacing in different directions in the illuminated area by the laser. These domains show many spots with identical diffraction diameters, forming Debye rings<sup>37,38</sup>. Furthermore, for a perfectly ordered 2DPC, the light is strongly forward diffracted at an angle and produces 6 bright diffraction spots, as shown in Fig. 2a. The particle spacing  $d$  can be calculated from the formula listed in Fig. 2b by measuring the Debye diffraction ring diameter  $D$ <sup>7</sup>. In this study, the laser wavelength  $\lambda$  was 532 nm, and the distance  $h$  between the 2DPC array plane and the bottom screen was set at 116 mm. Herein, the effect of the hydrogel thickness on the height  $h$  was neglected because the hydrogel thickness was on the micrometer level; the 116 mm  $h$  was 1000 times larger than the hydrogel thickness. In our study, we fabricated two hydrogel sensors with different thicknesses. The effect of the hydrogel thickness on the particle spacing of 2DPC hydrogel is discussed in detail in Section 3 in the Supporting Information. The results demonstrated that the differences in particle spacing for any one of the 2DPC hydrogel sensors with and without considering the hydrogel thickness were approximately 1 nm (Table S1). Therefore, we calculated the particle spacing of the hydrogel sensors without considering the hydrogel thickness.

For each particle spacing measurement, three 2DPC hydrogel samples were used for every experiment, and the  $d$  of each sample was measured at 3 different positions. From the 9 measurements, the average of  $d$  was calculated.

### Fabrication of TB-sensitive 2DPC hydrogel aptasensors

An equilibrated 2DPC hydrogel film was cut into pieces of 1 cm × 1 cm to modify the DNA aptamers. In detail, a piece

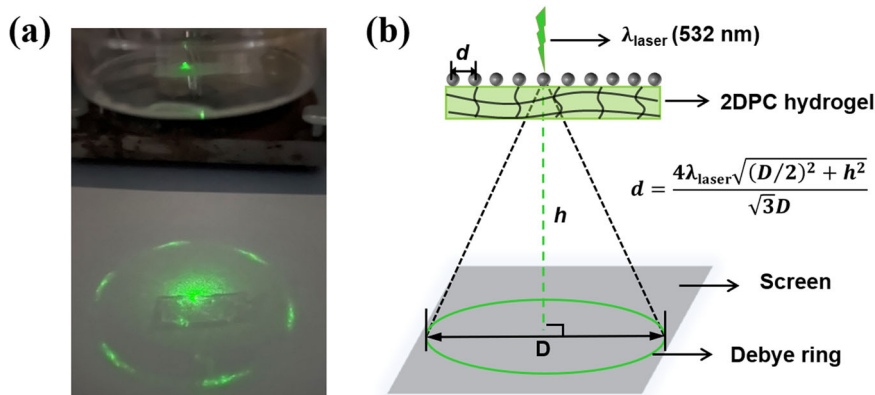


**Fig. 2 Measurement of Debye diffraction ring.** **a** Photograph of Debye ring diffracted by a 2DPC hydrogel and **b** Debye ring diameter measurement. The 2DPC was illuminated along the array normal by a 532 nm green laser pointer, producing a Debye diffraction ring on the bottom screen. The particle spacing  $d$  of the 2DPC was calculated from the formula  $d = \frac{4\lambda_{\text{laser}}\sqrt{(D/2)^2 + h^2}}{\sqrt{3}D}$ , where  $\lambda_{\text{laser}}$  is the laser wavelength,  $D$  is the diameter of the Debye ring, and  $h$  is the distance between the 2DPC array plane and the bottom screen.

of 2DPC film was immersed in 1 mL of PBS solution containing 15 mg EDC and 3 mg NHS for 1 h<sup>14,39</sup>, followed by PBS washing for 6 min (PBS was changed every 2 min). Then, 20  $\mu\text{L}$  of S1 solution and 10  $\mu\text{L}$  of S2 solution at a certain concentration were dropped onto the 2DPC piece, and the reaction was kept at room temperature for 1 h and at 4 °C overnight. After washing with PBS for 6 h (PBS was changed every 2 h), the aptamer-functionalized 2DPC was obtained and stored in PBS before use. The photoinitiated copolymerization reaction of AAm and AAC and the subsequent modification of DNA aptamers are shown in Scheme S1 in the Supporting Information. FTIR spectra (Fig. 3) demonstrated that the DNA aptamers successfully modified the polymer chains of the hydrogel according to the new absorption peaks at 1561  $\text{cm}^{-1}$  (C=N and C=C stretching vibration of DNA)<sup>40</sup>, 1223  $\text{cm}^{-1}$  (the symmetric stretching vibration of O=P=O in DNA)<sup>41</sup>, 1034  $\text{cm}^{-1}$  (C-O stretching vibration of DNA backbone)<sup>42,43</sup> and 776  $\text{cm}^{-1}$  (the ring breathing vibration of DNA)<sup>44</sup>. To simplify spectral analysis, the infrared samples were hydrogels that did not contain photonic crystals. In addition, aqueous solution was used in the whole preparation and modification process of the hydrogel to avoid the influence of the P=O groups in the PBS solution.

We adjusted the contents of AAC and Bis in the polymerizable precursor solutions and the concentrations of aptamers S1 and S2 to optimize the 2DPC biosensor, in which 110  $\mu\text{L}$  of precursor solution was used. Table 1 provides the compositions of the polymerizable precursor solutions used to prepare the 2DPC hydrogels. Herein, the prepared 2DPC films from the modification of S1 and S2 are denoted as S1/S2-2DPC. Using the same method, we fabricated aptamer S1- or S2-modified 2DPC films as

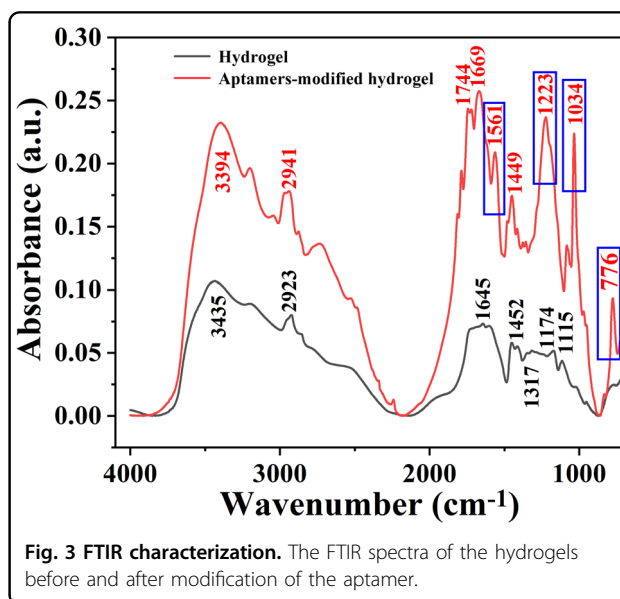


**Fig. 3 FTIR characterization.** The FTIR spectra of the hydrogels before and after modification of the aptamer.

control samples by adding 110  $\mu\text{L}$  of polymerizable precursor solution and denoted them as S1-2DPC and S2-2DPC, respectively. To study the influence of the hydrogel thickness on the detection performance, we prepared two S1/S2-2DPC films by changing the volumes of the precursor solution (110  $\mu\text{L}$  and 70  $\mu\text{L}$ ). The resultant 2DPC aptasensors are denoted as S1/S2-2DPC-110 and S1/S2-2DPC-70, respectively. Herein, the contents of AAm, AAC and Bis in the precursor solutions were 8.0 wt%, 3.0 wt% and 0.4 wt%, respectively, and 100  $\mu\text{M}$  S1 and S2 aptamers were used to perform the modification of the samples S1-2DPC, S2-2DPC, S1/S2-2DPC-110 and S1/S2-2DPC-70. The thicknesses of the hydrogels can be estimated by dividing the volume of

**Table 1** Compositions of polymerizable precursor solutions used to prepare 2DPCH.

Sample (#)	Total (g)	AAm (g)	AAc (g)	Bis (g)	H <sub>2</sub> O (g)	AAc (wt%)	Bis (wt%)
1	10	0.8	0.5	0.05	8.65	5	0.5
2			0.4	0.05	8.75	4	0.5
3			0.3	0.05	8.85	3	0.5
4			0.2	0.05	8.95	2	0.5
5			0.1	0.05	9.05	1	0.5
6			0.3	0.04	8.86	3	0.4
7			0.3	0.03	8.87	3	0.3
8			0.3	0.02	8.88	3	0.2

The precursor solutions were prepared by adding 20  $\mu\text{L}$  of 33% (w/v)  $\text{I}_{2959}$  in DMSO into 1 mL of polymerizable monomer solutions. Then, 110  $\mu\text{L}$  of the precursor solution was added onto the surface of a 2DPC array (2.4 cm  $\times$  3.2 cm) to prepare a 2DPCH. Then, 100  $\mu\text{M}$  DNA aptamers were used for the next modification.

the added precursor solution by the area of the glass slide containing the photonic crystal, ignoring the influence of the PS microsphere diameter. Therefore, the thicknesses were  $\sim 143 \mu\text{m}$  and  $\sim 91 \mu\text{m}$  for the hydrogels when the added precursor solutions were 110  $\mu\text{L}$  and 70  $\mu\text{L}$ , respectively.

#### Detection of TB in PBS solution and human serum

A 2DPCH film (1.0 cm  $\times$  1.0 cm) was immersed into TB solution (40  $\mu\text{L}$ ) prepared with PBS for a certain time, followed by thorough rinsing with PBS solution for more than 2 h (the PBS was changed every 30 min) before performing Debye diffraction ring measurements. The particle spacing changes of the photonic hydrogel aptasensor before and after reaction with TB solution were calculated to monitor the responsivity of the 2DPCH film.

Human serum was diluted 10-fold with PBS. Different concentrations of TB were spiked into the diluted serum solutions and used as the testing solutions. Pieces of the S1/S2-2DPCH films were immersed into 40  $\mu\text{L}$  of the testing solutions, and the particle spacing changes were recorded.

## Results and discussion

### Morphology of the 2DPCH

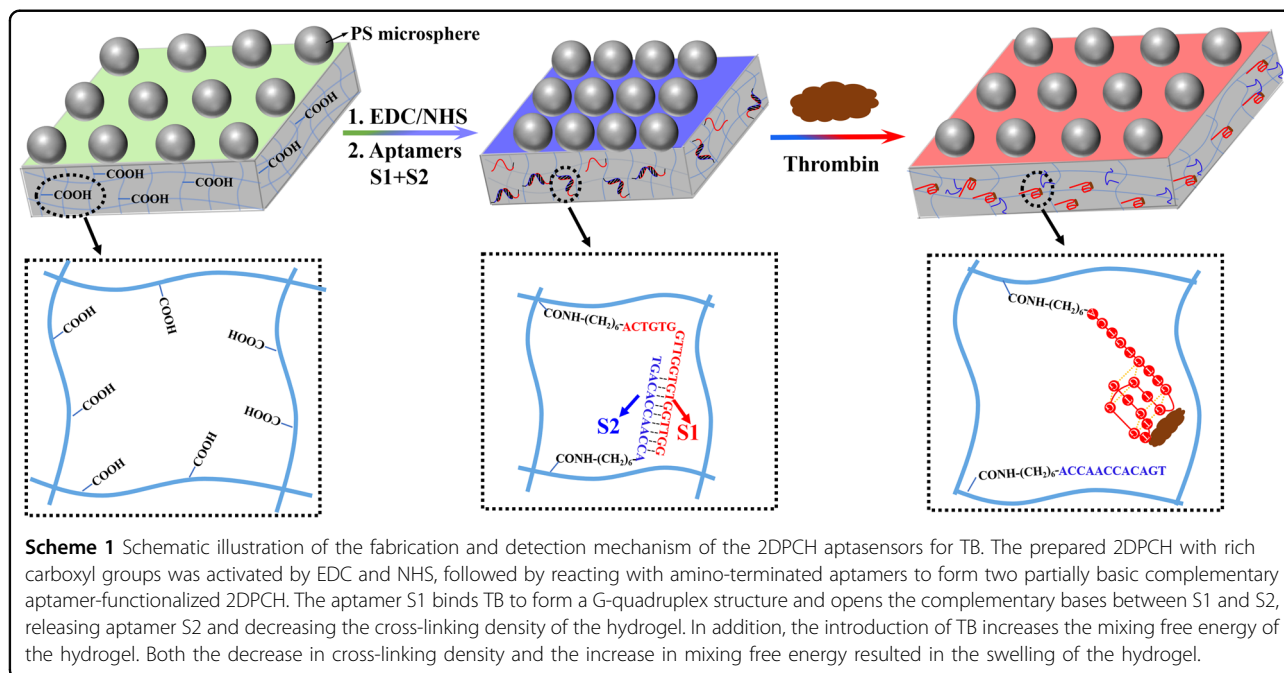
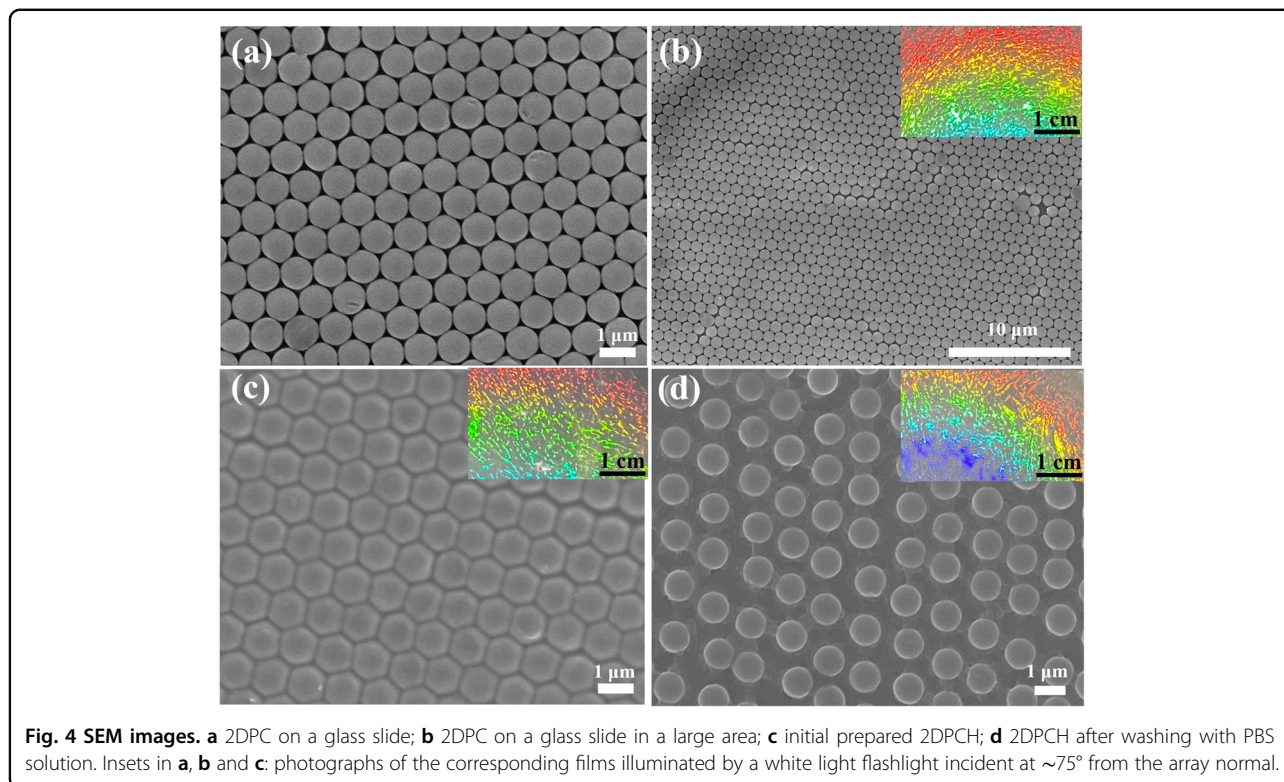
Figure 4a, b shows SEM images of the prepared PS 2DPC array on a glass side. The 2DPC exhibited a highly ordered and periodically arranged hexagonal close-packed structure over a large area and showed an iridescent color (Fig. 4b inset). The ordered 2DPC films provided an excellent platform for the preparation of 2DPC hydrogels. After UV polymerization, the 2DPC was embedded into the P(AAm-co-AAc) hydrogel network, as shown in Fig. 4c. Obviously, the original periodic microstructure of the 2DPC was not destroyed during the UV polymerization and perfectly maintained the ordered close-packed arrangement. We also observed an iridescent hydrogel

film (Fig. 3c inset). After the 2DPCH was washed with PBS, the hydrogel swelled due to the hydrophilic carboxyl group, leading to a nonclose-packed arrangement of PS particles in the polymer network while still maintaining the highly ordered hexagonal structure and the rainbow color of the 2DPC (Fig. 4d).

### Response of the S1/S2-2DPCH-110 aptasensors to TB

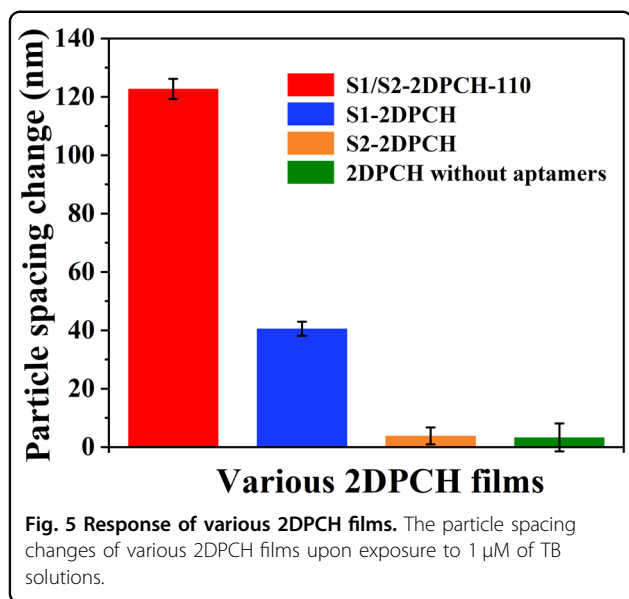
To investigate the detection feasibility of the prepared S1/S2-2DPCH-110 aptasensors for TB, the particle spacing changes of S1/S2-2DPCH-110, EDC-NHS-activated 2DPCH without aptamers and unactivated 2DPCH without aptamers were measured after exposure to 1  $\mu\text{M}$  TB solutions for 3 h. In addition, S1/S2-2DPCH-110 was also immersed into a blank PBS solution without TB, and the particle spacing change was recorded. The polymerizable precursor solutions for preparing these 2DPCH films had the same compositions (Table 1, sample 1). As shown in Fig. S2, the particle spacing of S1/S2-2DPCH-110 increased by  $88.04 \pm 6.04 \text{ nm}$  in the presence of 1  $\mu\text{M}$  TB, whereas the particle spacing changes of the other hydrogels under the same conditions were less than  $\sim 6 \text{ nm}$ . These results demonstrated that the constructed aptamer-modified 2DPCH biosensors showed a clear swelling response to TB, indicating that this 2DPCH film can be a candidate aptasensor for TB detection.

The response mechanism of the S1/S2-2DPCH-110 aptasensor for TB is shown in Scheme 1. The 2DPC-embedded P(AAm-co-AAc) hydrogel with rich carboxyl groups is activated by EDC and NHS and then reacts with amino-terminated DNA aptamers, which are linked to the polymer chains by amide bonds. The hydrogel shrinks after being modified by aptamers because the amino termini of aptamers S1 and S2 are linked to the polymer chains and simultaneously form complementary base pairs, which shorten the distance between the polymer chains<sup>45</sup>. Upon reacting with TB, the 2DPCH aptasensor



undergoes swelling due to the specific binding between the aptamer S1 and the TB molecules. Herein, aptamer S1 binds TB, and its single strand conformation changes into a G-quadruplex structure<sup>46</sup>. The complementary base pairs between S1 and S2 are opened, releasing aptamer S2

and increasing the distance between the polymer chains<sup>45</sup>. Thus, the binding between S1 and TB decreases the cross-linking density of the hydrogel, and as a result, the hydrogel swells after reaction with TB. In addition, both the conformational change of S1 and the introduction of



TB change the chemical structure of the hydrogel, leading to an increase in the mixing free energy<sup>3</sup>, which also induced the hydrogel to swell. Therefore, both the decrease in cross-linking density and the increase in mixing free energy cause the hydrogel to swell<sup>1,3</sup>.

To further confirm the detection mechanism of TB proposed in Scheme 1, we fabricated several 2DPCH films including S1/S2-2DPCH-110 (Table 1, sample 6), S1-2DPCH, S2-2DPCH and 2DPCH without aptamer. These hydrogel sensors were treated with 1  $\mu\text{M}$  TB for 3 h, and the resulting particle spacing changes are shown in Fig. 5. The particle spacing of S1/S2-2DPCH-110 increased by  $122.69 \pm 3.45$  nm, and that of S1-2DPCH increased by  $40.55 \pm 2.41$  nm. However, the particle spacing increases of S2-2DPCH- and nonaptamer-functionalized 2DPCH were lower than 4 nm, which could be negligible. The results demonstrated that only the 2DPCH films containing aptamer S1 could swell. This is due to the specific binding between S1 and TB. We also found that the particle spacing increase of S1/S2-2DPCH-110 was significantly larger than that of S1-2DPCH. There was an approximately 80 nm difference in the particle spacing change. This is because both the changes in cross-linking density and mixing free energy induced the swelling of the S1/S2-2DPCH-110 film, while only the increase in mixing free energy induced the swelling of the S1-2DPCH film. It can also be seen that the change in crosslinking density played a more important role in the swelling of the hydrogel. In brief, the decreased cross-linking density and increased mixing free energy of the hydrogel induced remarkable swelling and a particle spacing increase of more than 120 nm for the S1/S2-2DPCH-110 aptasensor.

#### Optimization of the S1/S2-2DPCH-110 aptasensors

To acquire a more sensitive 2DPCH aptasensor for TB, we first optimized the composition of the hydrogel precursor solutions. For S1/S2-2DPCH-110, AAc, as a functional monomer that provides carboxyl groups as the binding sites of aptamers, will influence the swelling and shrinkage ability of the hydrogels. Therefore, the content of AAc will be related to the response performance of the 2DPCH aptasensors. We fabricated a series of 2DPCH films by changing the amount of AAc: the polymerizable precursor solutions contained 8 wt% AAm and 0.5 wt% Bis, and the hydrogels were functionalized by 100  $\mu\text{M}$  S1 and S2 solutions (Table 1, samples 1–5). Figure 6a shows the particle spacing changes of these hydrogel sensors upon exposure to 1  $\mu\text{M}$  TB solution for 3 h. The particle spacing change increased from  $26.67 \pm 3.45$  nm to  $88.04 \pm 6.04$  nm when the AAc concentration ( $C_{\text{AAc}}$ ) increased from 1 wt% to 3 wt%. This is because an increase in the AAc content can provide more carboxyl groups to link more aptamers and to bind more TB, resulting in a larger particle spacing increase. A further increase in AAc concentration caused a decrease in the particle spacing change. This may be because too many hydrophilic carboxyl groups swelled the hydrogel too much, which limited its further swelling actuated by the binding between aptamer S1 and TB. Thus, 3 wt% AAc was subsequently used for preparing the S1/S2-2DPCH-110 films.

The content of the crosslinker (Bis) in the precursor solutions (Table 1, samples 3, 6–8.) was then adjusted for the hydrogel preparation, in which 8 wt% AAm, 3 wt% AAc and 100  $\mu\text{M}$  aptamer solutions were used. The resulting 2DPCH films reacted with 1  $\mu\text{M}$  TB solutions for 3 h. As seen in Fig. 6b, the particle spacing changes of these hydrogels sharply increased from  $70.64 \pm 3.68$  nm to  $124.57 \pm 4.44$  nm as the concentration of Bis ( $C_{\text{Bis}}$ ) increased from 0.2 wt% to 0.4 wt%. However, upon further increasing the Bis concentration to 0.5 wt%, the particle spacing change decreased to  $88.04 \pm 6.04$  nm. Obviously, S1/S2-2DPCH-110 prepared from 0.4 wt% Bis showed the largest particle spacing increase upon exposure to the same concentration of TB. The reason for this is that the hydrogel is liable to swell at a lower crosslinker content. The swelling ability will be inhibited at a higher concentration of crosslinker. Therefore, the 2DPCH films fabricated from 8 wt% AAm, 3 wt% AAc and 0.4 wt% Bis were used as optimal fundamental materials to construct the aptasensors of TB.

Aptamers, as recognition molecules, are key components of hydrogel biosensors, and the degree of their modification will undoubtedly influence the detection performance of the aptasensors<sup>13,22</sup>. Thus, the 2DPCH films prepared from the optimized polymerizable precursor solutions were modified with different concentrations of aptamers

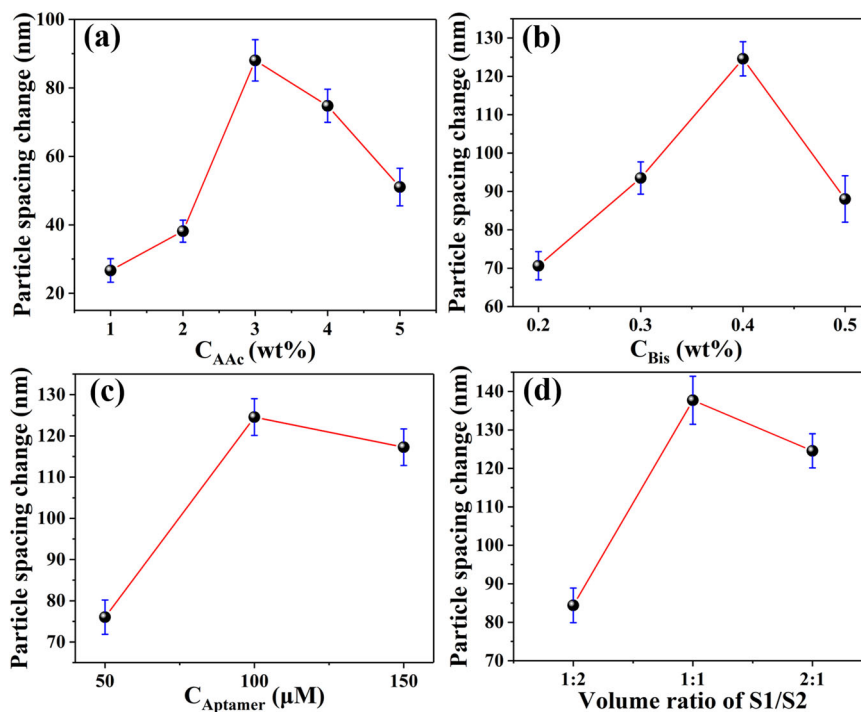


**Fig. 6 Optimization of the aptasensors.** Dependence of the particle spacing changes of the S1/S2-2DPCH-110 aptasensors on the concentrations of **a** AAC, **b** Bis and **c** aptamers and **d** the volume ratio of S1 (100  $\mu$ M) and S2 (100  $\mu$ M).

( $C_{Aptamer}$ ). The particle spacing changes after reacting with 1  $\mu$ M TB solution for 3 h are shown in Fig. 6c. The largest particle spacing increase of  $124.57 \pm 4.44$  nm was obtained from the 2DPCH aptasensor modified by 100  $\mu$ M aptamers. The particle spacing change decreased by 7.31 nm as the  $C_{Aptamer}$  concentration increased to 150  $\mu$ M. This may be attributed to the excessive amount of aptamer modification causing a higher crosslinking density of the hydrogel, which is not favorable for the swelling of the hydrogel.

Furthermore, we prepared three 2DPCH aptasensors modified by different volume ratios of S1 and S2, using 8 wt% AAm, 3 wt% AAC, 0.4 wt% Bis and 100  $\mu$ M S1 and S2. The particle spacing changes of these aptasensors after reacting with 1  $\mu$ M TB solutions for 3 h are given in Fig. 6d. The results showed that the particle spacing change increased from  $84.41 \pm 4.49$  nm to  $137.71 \pm 6.25$  nm when the volume ratio of S1/S2 changed from 1:2 (10  $\mu$ L S1, 20  $\mu$ L S2) to 1:1 (20  $\mu$ L S1, 20  $\mu$ L S2). This is because equivalent amounts of S1 and S2 are beneficial for forming more complementary pairs when modifying the hydrogel, resulting in a hydrogel aptasensor with a higher cross-linking density. After the response to TB, more binding between S1 and TB occurred, and more S2 was released, leading to the formation of a swollen hydrogel with a lower cross-linking density. We also found that the particle spacing change still reached  $124.57 \pm 4.44$  nm when the volume ratio of S1/S2 was set at

2:1 (20  $\mu$ L S1, 10  $\mu$ L S2). It only showed a difference of  $\sim 13$  nm compared with that from the volume ratio of 1:1. From an economic perspective, the 2DPCH aptasensors prepared with 8 wt% AAm, 3 wt% AAC, 0.4 wt% Bis, and 100  $\mu$ M (20  $\mu$ L S1, 10  $\mu$ L S2) aptamers were chosen as the sensors for detecting TB.

#### TB detection by the S1/S2-2DPCH-110 aptasensors

We investigated the response selectivity and anti-interference of the S1/S2-2DPCH-110 films toward TB by immersing the hydrogel sensors into 40  $\mu$ L of PBS solutions containing Cys, Lys, BSA, AD, and Alb, blank PBS solution and a mixture solution containing 1  $\mu$ M of these biomolecules for 3 h, respectively. The resulting particle spacing changes are shown in Fig. 7. The particle spacing of S1/S2-2DPCH-110 increased by  $122.69 \pm 3.45$  nm in TB solution and  $117.8 \pm 3.45$  4.79 nm in the mixture solution, whereas it increased less than  $13.82 \pm 2.59$  nm in the other biomolecule solutions and the blank solution. The significant difference in the particle spacing changes indicated that the constructed S1/S2-2DPCH-110 aptasensor had good selectivity and anti-interference for TB over the other biomolecules due to the specific binding between aptamer S1 and TB. A negligible particle spacing increase of  $3.32 \pm 4.75$  nm was obtained for the blank PBS solution, demonstrating TB-induced hydrogel swelling because of the existence of the TB-binding aptamer in the biosensor.



The dependence of the particle spacing changes of the S1/S2-2DPCH-110 aptasensors on the TB concentration ( $C_{TB}$ ) was studied to explore the detection sensitivity of this sensor to TB. As shown in Fig. 8a, the changes in particle spacing sharply increased from  $17.02 \pm 4.07$  nm to  $122.69 \pm 3.45$  nm with increasing TB concentration from

1 nM to 1  $\mu$ M and then leveled off. Furthermore, the magnitude of the particle spacing increase was linearly related to the logarithm of  $C_{TB}$  within 1–500 nM (Fig. 8b). The correlation coefficient ( $R^2$ ) was 0.9915, and the LoD was 0.82 nM ( $S/N = 3$ ).

To further improve the sensing performance of the aptasensor, we attempted to reduce the hydrogel thickness by decreasing the volume of the polymerizable precursor solution. To this end, the S1/S2-2DPCH aptasensors fabricated by using 70  $\mu$ L of precursor solutions (S1/S2-2DPCH-70) were immersed into different concentrations of TB solutions, and the resulting particle spacing increases were recorded, as shown in Fig. 8c. The change tendency of the particle spacing increase was similar to that of the S1/S2-2DPCH-110 fabricated from 110  $\mu$ L precursor solution. The particle spacing changes of S1/S2-2DPCH-70 also linearly increased with the logarithm of  $C_{TB}$  over the range of 1–500 nM with an  $R^2$  of 0.9957 (Fig. 8d), and the LoD was found to be 0.64 nM ( $S/N = 3$ ). These results demonstrated that reducing the hydrogel thickness can improve the detection sensitivity of the aptasensor for TB. In addition, S1/S2-2DPCH-70 also showed good selectivity and anti-interference for detecting TB (Fig. S3).

Figure 9a, b shows the time dependence of the particle spacing changes for the two 2DPCH aptasensors with different thicknesses at three different TB concentrations. The particle spacing changes of both of the hydrogel aptasensors

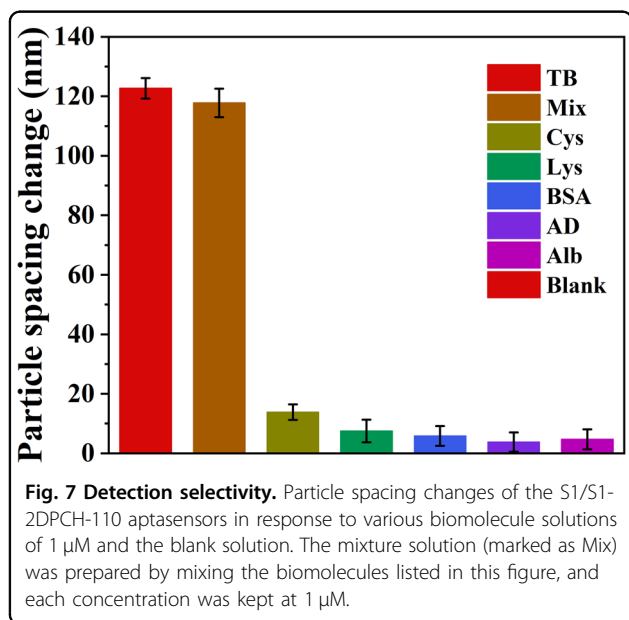


**Fig. 7 Detection selectivity.** Particle spacing changes of the S1/S2-2DPCH-110 aptasensors in response to various biomolecule solutions of 1  $\mu$ M and the blank solution. The mixture solution (marked as Mix) was prepared by mixing the biomolecules listed in this figure, and each concentration was kept at 1  $\mu$ M.

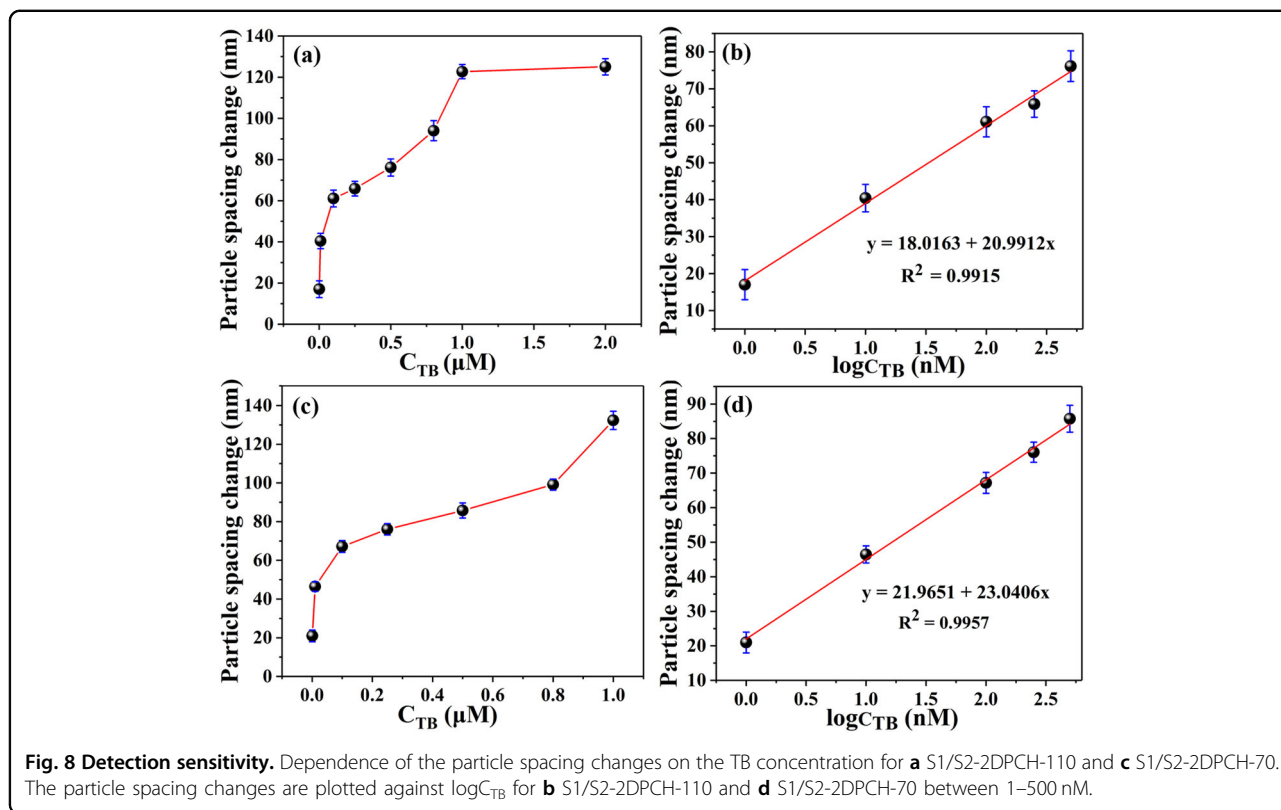


**Fig. 8 Detection sensitivity.** Dependence of the particle spacing changes on the TB concentration for **a** S1/S2-2DPCH-110 and **c** S1/S2-2DPCH-70. The particle spacing changes are plotted against  $\log C_{TB}$  for **b** S1/S2-2DPCH-110 and **d** S1/S2-2DPCH-70 between 1–500 nM.

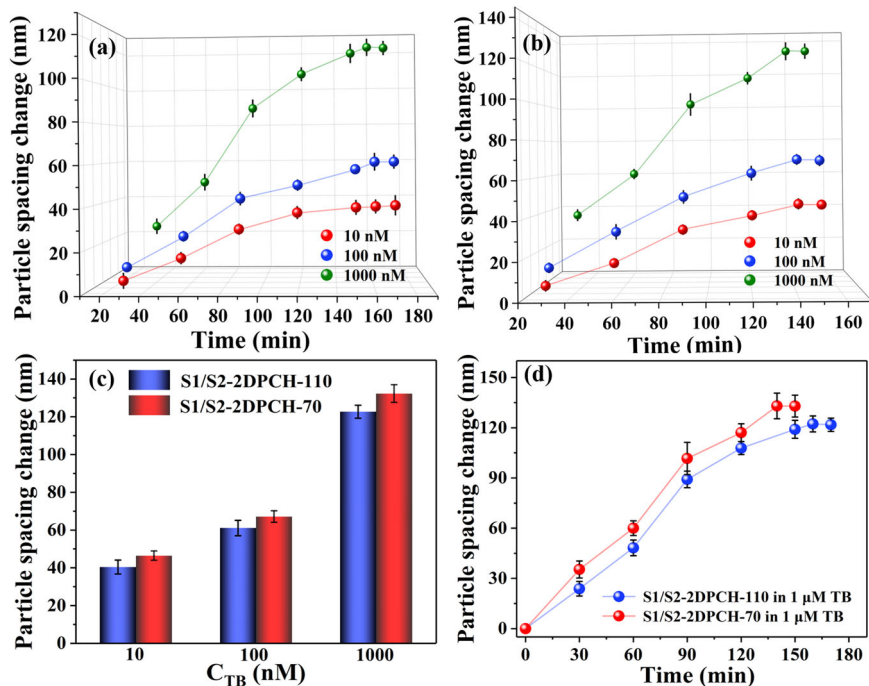


**Fig. 9** Particle spacing changes at different TB concentrations and times. Time dependence of the particle spacing changes for **a** S1/S2-2DPCH-110 and **b** S1/S2-2DPCH-70 when placed in different TB concentrations. **c** Particle spacing changes of these two aptasensors exposed to 10 nM, 100 nM and 1  $\mu$ M TB solutions. **d** Time dependence of the particle spacing changes for these two aptasensors exposed to 1  $\mu$ M TB solution.

**Table 2** Detection of TB in human serum.

Sample	Aptasensors	Added (nM)	Found (nM)	Recovery %	RSD % ( $n = 3$ )
Human serum	S1/S2-2DPCH-110	10	11.53	115.30%	1.20%
		100	103.51	103.51%	0.65%
		500	477.44	95.50%	1.30%
	S1/S2-2DPCH-70	10	10.42	104.21%	2.52%
		100	95.74	95.74%	6.58%
		500	486.08	97.22%	4.64%

increased rapidly within 90 min and then gradually increased and leveled off at any concentration. At lower TB concentrations (10 nM and 100 nM), the thicker hydrogel sensor S1/S2-2DPCH-110 needed 160 min to reach the maximal particle spacing change (Fig. 9a), while the thinner sensor S1/S2-2DPCH-70 needed 140 min (Fig. 9b). Obviously, the thinner hydrogel sensor took less time to reach the response equilibrium. Additionally, at the same TB concentration, S1/S2-2DPCH-70 showed a slightly larger particle spacing increase after reaching the response equilibrium, as shown in Fig. 9c and Fig. S4. Figure 9d further demonstrates that the thinner hydrogel aptasensor had a larger particle spacing increase after reacting for the same time with the same concentration of TB, indicating a more

sensitive volume change and a faster response. The above results showed that reducing the thickness of the hydrogel sensor is beneficial for improving its response performance.

#### TB detection in human serum

Both the S1/S2-2DPCH-110 and S1/S2-2DPCH-70 aptasensors were used to detect TB in human serum by the standard addition method. Various concentrations (10 nM, 100 nM and 500 nM) of TB in 10-fold diluted human serum were tested, and the particle spacing changes before and after response were recorded. According to the linear relationships shown in Figs. 8b and 8d, we calculated the TB concentration in each human serum testing solution, as shown in Table 2.

S1/S2-2DPCH-110 showed good recoveries for detecting TB in human serum from 95.50% to 115.30%, and the relative standard deviation (RSD) was 0.65–1.30%. Moreover, S1/S2-2DPCH-70 also exhibited good recoveries of 95.74–104.21% and RSDs of 2.52–6.58%. The results demonstrated that the constructed photonic hydrogel aptasensor can be well applied in TB detection in human serum, showing promise for the development of home kits.

## Conclusion

Thrombin-sensitive smart photonic hydrogel aptasensors were constructed by modifying 2DPC-embedded P(AAm-co-AAc) hydrogels with complementary aptamers S1 and S2. In the presence of TB, aptamer S1 specifically bound TB, opening the complementary components of S1 and S2 and resulting in a decrease in the cross-linking density of the hydrogel. Additionally, when TB entered the hydrogel by binding with aptamer S1, the mixing free energy of the hydrogel increased. Both the decrease in cross-linking density and increase in the mixing free energy of the hydrogel caused the 2DPCH aptasensor to undergo swelling. The swelling of the photonic hydrogel aptasensor was monitored by measuring the Debye diffraction ring to acquire the particle spacing changes. The optimized S1/S2-2DPCH aptasensor showed a particle spacing increase of more than 120 nm. The aptamer-functionalized 2DPCH sensors could detect TB with high selectivity and sensitivity, and an LoD of 0.64 nM was obtained by further adjusting the thickness of the hydrogel. The constructed hydrogel aptasensor was successfully used to detect TB in human serum with recoveries of 95.74–104.21% and RSDs of 2.52–6.58%. This type of 2DPCH aptasensor is simple to operate and has easily readable optical signals. It provides a new method for the construction of photonic hydrogel aptasensors with other chemical or biological molecules by modifying the corresponding binding aptamers and has the potential to be developed into home kits.

## Acknowledgements

The authors thank the National Natural Science Foundation of China (Grant No. 21663032 and 22061041) and the Open Sharing Platform for Scientific and Technological Resources of Shaanxi Province (Grant No. 2021PT-004) for financial support.

## Author contributions

P.S.: Methodology, data curation, formal analysis, validation, writing-original draft. M.L.: Data curation, validation. R.L.: Investigation, formal analysis, writing – review and editing. B.H., H.M., and X.H.: Investigation and formal analysis. Y.Z.: Resources, conceptualization, writing – review and editing, supervision, project administration, funding acquisition. J.-J. W.: Writing – review & editing.

## Data availability

Data supporting the findings of this study are available from the corresponding author upon request.

## Competing interests

The authors declare no competing interests.

## Publisher's note

Springer Nature remains neutral with regard to jurisdictional claims in published maps and institutional affiliations.

**Supplementary information** The online version contains supplementary material available at <https://doi.org/10.1038/s41427-022-00443-y>.

Received: 26 June 2022 Revised: 17 September 2022 Accepted: 22 September 2022.

Published online: 9 December 2022

## References

- Shen, P. et al. Three-dimensional/two-dimensional photonic crystal hydrogels for biosensing. *J. Mater. Chem. C* **9**, 5840–5857 (2021).
- Wang, Y., Zhang, D., Zhang, H., Shang, L. & Zhao, Y. Responsive photonic alginate hydrogel particles for the quantitative detection of alkaline phosphatase. *NPG Asia Mater.* **14**, 54 (2022).
- Cai, Z., Smith, N. L., Zhang, J.-T. & Asher, S. A. Two-dimensional photonic crystal chemical and biomolecular sensors. *Anal. Chem.* **87**, 5013–5025 (2015).
- Cai, Z. et al. From colloidal particles to photonic crystals: advances in self-assembly and their emerging applications. *Chem. Soc. Rev.* **50**, 5898–5951 (2021).
- Tikhonov, A. Reflectivity enhanced two-dimensional dielectric particle array monolayer diffraction. *J. Nanophotonics* **6**, 063509 (2012).
- Zhang, J.-T., Chao, X., Liu, X. & Asher, S. A. Two-dimensional array Debye ring diffraction protein recognition sensing. *Chem. Commun.* **49**, 6337–6339 (2013).
- Cai, Z. et al. 2D photonic crystal protein hydrogel coulometer for sensing serum albumin ligand binding. *Anal. Chem.* **86**, 4840–4847 (2014).
- Li, X. et al. Redox/temperature responsive nonionic nanogel and photonic crystal hydrogel: Comparison between N, N'-Bis(acryloyl)cystamine and N, N'-methylenebisacrylamide. *Polymer* **137**, 112–121 (2018).
- Cao, Y. et al. A sulfamethoxazole molecularly imprinted two-dimensional photonic crystal hydrogel sensor. *Soft Matter* **17**, 4969–4978 (2021).
- Zheng, B., Liu, G., Zhao, L., Wang, G. & Wang, Y. Levofloxacin molecularly imprinted two dimensional photonic crystal hydrogel sensor. *Polymer* **239**, 124448 (2022).
- Cao, Y., Liu, G., Qin, X., Li, H. & Liu, C. Preparation and application of 2-chlorophenol molecularly imprinted photonic crystal hydrogel sensor. *J. Macromol. Sci. A* **58**, 336–343 (2021).
- Liu, R. et al. Colorimetric two-dimensional photonic crystal biosensors for label-free detection of hydrogen peroxide. *Sens. Actuat. B- Chem.* **354**, 131236 (2022).
- Chen, Q. et al. Construction and research of multiple stimuli-responsive 2D photonic crystal DNA hydrogel sensing platform with double-network structure and signal self-expression. *Anal. Chem.* **94**, 5530–5537 (2022).
- Li, G. et al. Label-free 2D colloidal photonic crystal hydrogel biosensor for urea and urease inhibitor. *Sens. Actuat. B- Chem.* **277**, 591–597 (2018).
- Li, W., Xiang, J., Men, D. & Zhang, H. 2D Au nanosphere arrays/PVA-PBA-modified-hydrogel composite film for glucose detection with strong diffraction intensity and linear response. *Nanomaterials* **9**, 140 (2019).
- Yan, Z. et al. A non-enzymatic urine glucose sensor with 2-D photonic crystal hydrogel. *Anal. Bioanal. Chem.* **408**, 8317–8323 (2016).
- Wang, C., Li, F., Bi, Y. & Guo, W. Reversible modulation of 2D photonic crystals with a responsive shape-memory DNA hydrogel film. *Adv. Mater. Interfaces* **6**, 1900556 (2019).
- Cai, Z., Sasmal, A., Liu, X. & Asher, S. A. Responsive photonic crystal carbohydrate hydrogel sensor materials for selective and sensitive lectin protein detection. *ACS Sens.* **2**, 1474–1481 (2017).
- Zhang, J.-T., Cai, Z., Kwak, D. H., Liu, X. & Asher, S. A. Two-dimensional photonic crystal sensors for visual detection of Lectin Concanavalin A. *Anal. Chem.* **86**, 9036–9041 (2014).
- Cai, Z. et al. A photonic crystal protein hydrogel sensor for *Candida albicans*. *Angew. Chem. Int. Ed.* **54**, 13036–13040 (2015).
- Murtaza, G. et al. Glycated albumin based photonic crystal sensors for detection of lipopolysaccharides and discrimination of Gram-negative bacteria. *Anal. Chim. Acta* **1117**, 1–8 (2020).

22. Murtaza, G., Rizvi, A. S., Xue, M., Qiu, L. & Meng, Z. Consensus receptor-binding domain-targeted aptamer selection and designing of a photonic crystal-decorated aptasensor for SARS-CoV-2. *Anal. Chem.* **94**, 7391–7399 (2022).
23. Vízovišek, M. et al. Protease specificity: towards in vivo imaging applications and biomarker discovery. *Trends Biochem. Sci.* **43**, 829–844 (2018).
24. Akiyama, H., Ikeda, K., Kondo, H. & McGeer, P. L. Thrombin accumulation in brains of patients with Alzheimer's disease. *Neurosci. Lett.* **146**, 152–154 (1992).
25. Waller, A. P., Nieman, M. T., Smoyer, W. E. & Kerlin, B. A. Endogenous thrombin potential is directly correlated with proteinuria severity in both nephrotic syndrome patients and an animal model of nephrotic syndrome. *Blood* **124**, 4243–4243 (2014).
26. Tripodi, A. et al. The endogenous thrombin potential and the risk of venous thromboembolism. *Thromb. Res.* **121**, 353–359 (2007).
27. Reddel, C., Tan, C. & Chen, V. Thrombin generation and cancer: contributors and consequences. *Cancers* **11**, 100 (2019).
28. Urbanová, V. et al. Hierarchical porous fluorinated graphene oxide@metal-organic gel composite: label-free electrochemical aptasensor for selective detection of thrombin. *ACS Appl. Mater. Interfaces* **10**, 41089–41097 (2018).
29. Kotlarek, D. et al. Surface plasmon resonance-based aptasensor for direct monitoring of thrombin in a minimally processed human blood. *Sens. Actuat. B- Chem.* **320**, 128380 (2020).
30. Jiang, N., Zhu, T. & Hu, Y. Competitive aptasensor with gold nanoparticle dimers and magnetite nanoparticles for SERS-based determination of thrombin. *Microchim. Acta* **186**, 747 (2019).
31. Nimjee, S. M., White, R. R., Becker, R. C. & Sullenger, B. A. Aptamers as therapeutics. *Annu. Rev. Pharmacol. Toxicol.* **57**, 61–79 (2017).
32. Bock, L. C., Griffin, L. C., Latham, J. A., Vermasas, E. H. & Toole, J. J. Selection of single-stranded DNA molecules that bind and inhibit human thrombin. *Nature* **355**, 564–566 (1992).
33. Liu, J., Cao, Z. & Lu, Y. Functional nucleic acid sensors. *Chem. Rev.* **109**, 1948–1998 (2009).
34. Xiong, X. et al. Responsive DNA-based hydrogels and their applications. *Macromol. Rapid Commun.* **34**, 1271–1283 (2013).
35. Zhang, F., Cao, L. & Yang, W. Preparation of monodisperse and anion-charged polystyrene microspheres stabilized with polymerizable sodium styrene sulfonate by dispersion polymerization. *Macromol. Chem. Phys.* **211**, 744–751 (2010).
36. Zhang, J.-T., Wang, L., Lamont, D. N., Velankar, S. S. & Asher, S. A. Fabrication of large-area two-dimensional colloidal crystals. *Angew. Chem. Int. Ed.* **124**, 6221–6224 (2012).
37. Lumsdon, S. O., Kaler, E. W. & Velev, O. D. Two-dimensional crystallization of microspheres by a coplanar AC electric field. *Langmuir* **20**, 2108–2116 (2004).
38. Pan, F., Zhang, J., Cai, C. & Wang, T. Rapid fabrication of large-area colloidal crystal monolayers by a vortical surface method. *Langmuir* **22**, 7101–7104 (2006).
39. Ye, B.-F. et al. Colorimetric photonic hydrogel aptasensor for the screening of heavy metal ions. *Nanoscale* **4**, 5998 (2012).
40. Mao, Y., Daniel, L. N., Whittaker, N. & Saffioti, U. DNA binding to crystalline silica characterized by Fourier-transform infrared spectroscopy. *Environ. Health Persp.* **102**, 7 (1994).
41. Thomas, L. C. & Chittenden, R. A. Characteristic infrared absorption frequencies of organophosphorus compounds—I The phosphoryl (P=O) group. *Spectrochim. Acta A* **20**, 467–487 (1964).
42. Babić, S. D. & Serec, K. Sodium and manganese salt DNA thin films: An infrared spectroscopy study. *Spectrochim. Acta A* **241**, 118646 (2020).
43. Tohidi Moghadam, T. & Ranjbar, B. Heat induced aggregation of gold nanorods for rapid visual detection of lysozyme. *Talanta* **144**, 778–787 (2015).
44. Muntean, C. M. et al. The influence of UV femtosecond laser pulses on bacterial DNA structure, as proved by Fourier Transform Infrared (FT-IR) spectroscopy. *ChemistrySelect* **6**, 6957–6972 (2021).
45. Wang, X. & Wang, X. Aptamer-functionalized hydrogel diffraction gratings for the human thrombin detection. *Chem. Commun.* **49**, 5957 (2013).
46. Zhang, Q. et al. Electrochemical sandwich-type thrombin aptasensor based on dual signal amplification strategy of silver nanowires and hollow Au-CeO<sub>2</sub>. *Biosens. Bioelectron.* **150**, 111846 (2020).